Heat Transfer and Fluid Flow Over Circular Cyclinders in Cross Flow

[1]M. JIBRAN HAIDER*, S. NOMAN DANISH, W. A. KHAN, S. UZAIR MEHDI & BILAL AHMED ABBASI

[1]Department of Engineering SciencesNational University of Sciences and Technolo (NUST)
Pakistan Navy Engineering College (PNEC), Karachi
*jibranhaider@hotmail.com

NUST Journal of Engineering Sciences, Vol.3, No.1 , Dec 2010

Abstract

An extensive numerical study is conducted to determine cross flow of air (Pr=0.71) around isothermal cylinders of circular cross-section in arrangements such as single cylinder, inline arrays and staggered arrays. Commercial software package FLUENT is used to solve the fluid flow and energy equations assuming the flow over the cylinder is two dimensional, steady, viscous and incompressible bounded in a duct, as low Reynolds number is being investigated. The width of the duct is kept 20 times the diameter of the cylinder so that the effects of channel blockage can be avoided. The effects of radiation are also neglected in this study. Variations in properties such as local Nusselt number, average Nusselt number, local pressure coefficient and local skin friction coefficient are presented around the cylinders at Reynolds number ranging from 40 to 10,000. The results are compared with analytical, experimental and numerical data from previous literature and are found to be in excellent agreement. It has been found that heat transfer from a staggered array of cylinders is slightly higher than an inline array of cylinders.

Keywords: Heat Transfer; Computational Fluid Dynamics; FLUENT; Reynolds Number; Nusselt Number; Circular Cylinder

Nomenclature

B.C	Boundary condition
CFD	Computational Fluid Dynamics
Cp	Specific heat at constant pressure [J/kg.K]
Cp (θ)	Local pressure coefficient, $C_p(\theta) = p(\theta) - p(\infty)/0.5\rho U_\infty^2$
D	Diameter of the cylinder [m]
h (θ)	Local heat transfer coefficient [W/m2.K]
k	Thermal conductivity [W/m.K]
L	Characteristic length = Diameter of cylin der [m]
Nu_L	Average Nusselt number based on char- acte ristic length, $Nu=hL/k$
Nu_L (θ)	Local Nusselt number, $Nu_L(\theta) = h(\theta)L/k$
p (θ)	Local static pressure at the surface of cylinder [N/m2]
P∞	Free stream pressure [N/m2]
Pr	Prandtl number, $Pr = \mu c_p/k$
ReL	Reynolds number based on characteristic length, $Re = \rho U_\infty L/\mu$
T	Temperature [K]
Tw	Wall temperature [K]
T∞	Free stream temperature [K]
u	x component of velocity [m/s]
U∞	Free stream velocity [m/s]
v	y component of velocity [m/s]
W	Width of duct [m]

Greek Symbols

θ	Angular displacement measured clockwise from front stagnation point [°]
μ	Dynamic viscosity [kg/m.s]
ρ	Density [kg/m3]

Corresponding Author: M. JibranHaider (NJES10030131)

NUST Journal of Engineering Sciences, Vol.3, No.1 , Dec 2010

Introduction

Investigation of heat transfer and fluid flow around cylinders has been a popular subject because of its importance in variety of applications such as heat exchangers, nuclear reactors, overhead cables, power generators, thermal apparatus, etc. Many researchers have analytically, experimentally and numerically determined heat transfer and flow structures around circular cylinders placed in a bank and as well as in isolation. A brief summary is provided below.

An extensive analytical study has been carried out by Van Der Hegge [1] to produce a new correlation formula to determine heat transfer by natural and forced convection from horizontal cylinders. Similarly, Refai Ahmed & Yovanovich [2] have developed a method to determine heat transfer by forced convection from isothermal bodies such as infinite circular cylinders, flat plates and spheres. The solution is valid for a wide range of Reynolds and Prandtl numbers. More recently Khan et al. [3] [4] have investigated fluid flow and heat transfer from a single circular cylinder and an infinite circular cylinder analytically by the Von Karman –Pohlhausen method. Correlations are obtained for heat transfer and drag coefficients which are applicable for a wide range of Reynolds and Prandtl numbers. Effects of both isothermal and isoflux boundary conditions are analyzed.

Meel [5] experimentally determined the circumferential heat transfer coefficient by measuring temperature distribution on the outer surface of the cylinder. A series of experiments were conducted by Igarashi [6] [7] at high Reynolds Numbers to determine pressure and drag coefficients around two circular cylinders placed in tandem. The effects of varying the longitudinal distance between the cylinders and their diameters were also investigated. Igarashi along with Suzuki [8] extended the study to three circular cylinders arranged inline. An extensive experimental study was undertaken by Buyruk [9] to determine local Nusselt Number and local pressure coefficient around a circular cylinder for various Reynolds Numbers and blockage ratios. This research was also extended to tube banks and the variation of local Nusselt Number was obtained for every row with changes in longitudinal and transverse pitches. Similarly Mehrabian [10] attempted to investigate the rate of cooling of a cylindrical copper element by forced convection. The author has also analyzed the uncertainty in the measurement of heat transfer characteristics of the system. On the other hand, Wung and Chen [11] have utilized a finite analytic method to determine heat transfer at various Reynolds numbers from inline and staggered tube arrays. Buyruk [12] has numerically investigated heat transfer from cylinders placed in tandem, inline tube banks and staggered tube banks. He has used a finite element method to obtain the circumferential variation in Nusselt number for the cylinders. A steady as well as an unsteady analysis has been undertaken by Szczepanik et al. [13] to determine heat transfer from a cylinder in cross flow. Unsteady simulations of the cylinder depict vortex shedding. The numerical study makes use of a k-ω turbulence model.

The present study utilizes a commercial CFD software package, FLUENT which is based on a control volume based technique to solve the governing equations such as conservation of mass, momentum, energy and turbulence. Algebraic equations are generated for discrete dependant variables like pressure, velocity, temperature etc, for each control volume. Finally the discretized equations are linearized and a solution is obtained [14].

Computational Methods

A. Methodology

The following methodology has been adopted in order to obtain results through CFD simulations. It highlights the iterative procedure which must be carried out in order to obtain an accurate set of results.

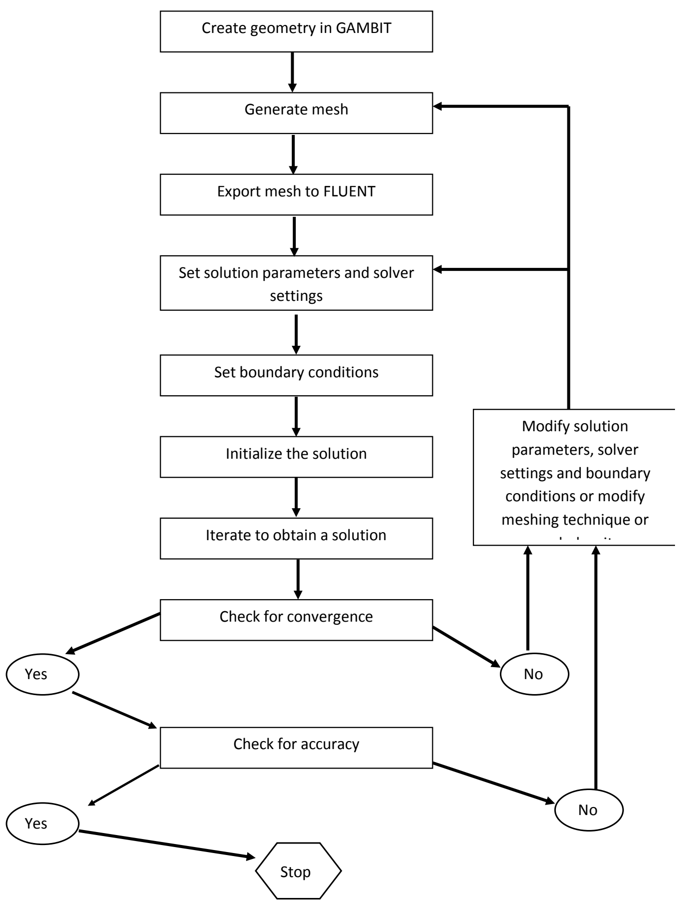

B. Assumptions

A two dimensional analysis is performed as the length of the cylinder is kept much greater than its diameter. The assumption that flow is incompressible is warranted as relatively low Reynolds number is being investigated. The width of the duct is kept much larger (20 times) than the diameter of the cylinder so that the wall effects of the duct can be neglected. This means that the effects of boundary layer formation on the duct boundary will not affect the flow in the vicinity of the cylinder.

C. Geometry and Meshing

The geometry is created in GAMBIT, which is the pre-processor for geometric modeling and mesh generation. The rectangular computational domain is bounded by the inlet, outlet and duct boundaries. The flow enters the domain from the inlet boundary on the extreme left and leaves from the outlet boundary on the extreme right for all simulations. A 2D structured mesh of non uniform grid spacing is created. The mesh density is kept intense near the cylinder for resolving the boundary layer accurately. The distinct points of the mesh are called nodes where all the equations involved in the system are solved. These equations are:

Equation of continuity

$$\frac{\partial u}{\partial x}+\frac{\partial v}{\partial y}=0$$

x component of conservation of momentum

$$\frac{\partial u}{\partial t}+u\frac{\partial u}{\partial x}+v\frac{\partial u}{\partial y}=-\frac{1}{\rho}\frac{\partial p}{\partial x}+\frac{\mu}{\rho}\left(\frac{\partial^2 u}{\partial x^2}+\frac{\partial^2 u}{\partial y^2}\right)$$

y component of conservation of momentum

$$\frac{\partial v}{\partial t}+u\frac{\partial v}{\partial x}+v\frac{\partial v}{\partial y}=-\frac{1}{\rho}\frac{\partial p}{\partial y}+\frac{\mu}{\rho}\left(\frac{\partial^2 v}{\partial x^2}+\frac{\partial^2 v}{\partial y^2}\right)$$

Energy equation

$$\frac{\partial T}{\partial t}+u\frac{\partial T}{\partial x}+v\frac{\partial T}{\partial y}=\alpha\left(\frac{\partial^2 T}{\partial x^2}+\frac{\partial^2 T}{\partial y^2}\right)$$

Basically two slightly different techniques were utilized for mesh generation. The first technique was applied to the mesh of a single cylinder. It involves the generation of a block structured quadrilateral mesh around the cylinder. Figure 1 focuses on the mesh in the vicinity of a circular cylinder. It highlights the block technique which is used for a smooth transition in mesh. A smooth transition in cell volumes between adjacent cells is necessary as inability to do so may lead to truncation errors.

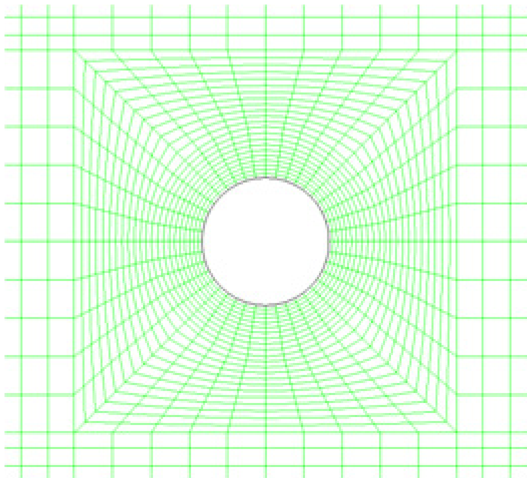

Figure 1: Mesh in the Vicinity of the Cylinder

The second technique of mesh generation is applied to inline and staggered arrangements. The mesh for these arrangements consists of tri meshing. Due to a relatively complex geometry generating block, structured quadrilateral mesh near the cylinders is time consuming and therefore not feasible. The mesh is shown below.

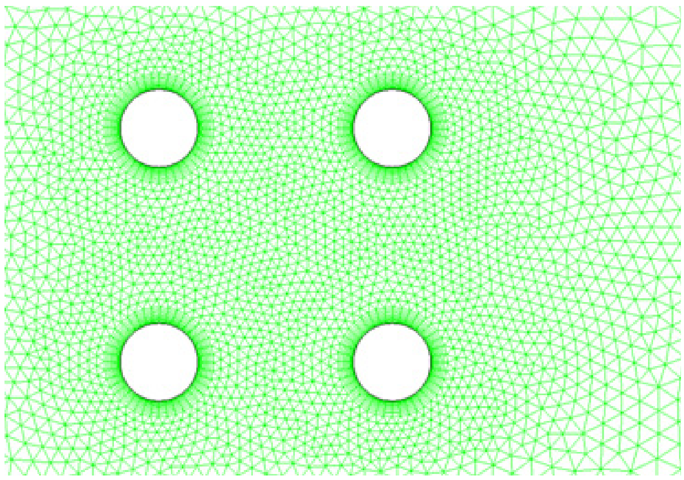

Figure 2: Mesh in the Vicinity of Four Cylinders placed in an Inline Array

D. Solver Settings

All numerical simulations are performed under the double precision solver as opposed to the single precision solver. The double precision solver performs

NUST Journal of Engineering Sciences, Vol.3, No.1 , Dec 2010

Corresponding Author: M. JibranHaider (NJES10030131)

better where pressure differences are involved and high convergence with accuracy is demanded [14]. A pressure-based solver which in previous versions of FLUENT was referred as the segregated solver was selected, as the present study deals with an incompressible flow. A second order upwind scheme was used to discretize the convective terms in the momentum and energy equations. This scheme though is time-consuming but it yields an accurate solution. This high order accuracy is achieved by a Taylor series expansion about the cell centroid [14]. A convergence criterion of 10^{-6} was found sufficiently accurate for this study and was applied to all residuals except energy for which the criterion was extended to 10^{-9}.

E. Boundary Conditions

Following boundary conditions were applied to the boundaries for all cases.

- Inlet Boundary: A velocity inlet boundary condition is applied to the inlet boundary as it is intended for incompressible flows. A uniform velocity profile is defined normal to the inlet boundary
- Outlet Boundary: An outflow boundary condition is employed at the outlet boundary. Its use is justified as the flow velocity and pressure at the outlet are unknown before the solution of the problem. It works on the principle of zero diffusion flux normal to the outflow boundary for all variables except pressure. It merely extrapolates information from within the domain and applies to the outlet without disturbing the upstream flow [14].
- Cylinder: A wall boundary condition is selected for the isothermally heated cylinder. The cylinder is heated to a temperature of 400 K for all simulations. In addition, a no slip condition is employed along the cylinder surface.
- Duct Boundary: The fluid flow is bounded within the duct by applying the wall boundary and no slip condition.

The mesh with dimensions and boundary conditions is shown in the figure below. It is to be noted that the actual mesh is much finer than the one shown.

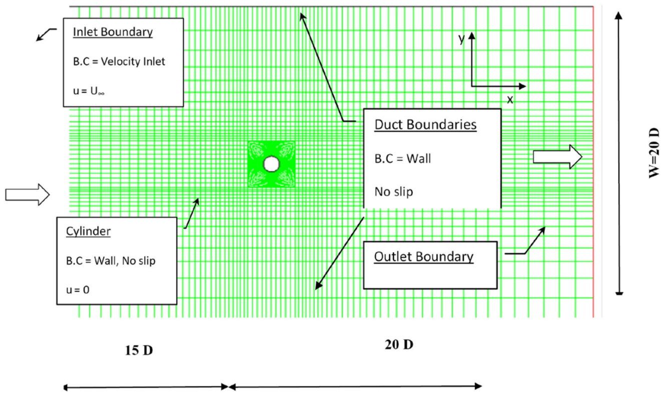

Figure 3: Meshed Computational Domain with Boundary Conditions

F. Grid Independence Study

In order to study the effect of grid size on the results, meshes of three different densities were created, solved and their results were analyzed. The following table shows the details of grid sizes for flow over a single circular cylinder and the corresponding effects on the average Nusselt number at a Reynolds number of 100. The results were found to be grid independent beyond the "average" mesh size.

Table 1

Effect of Grid Size on Average Nusselt Number

	Mesh Size	No. of Nodes	Average Nusselt No	Percentage Error
1.	Coarse	4120	5.2513	--
2.	Average	14260	5.1513	1.90
3.	Fine	37220	5.1401	0.22

Results and Discussion

A. Flow over a Single Cylinder

- **Average Nusselt Number**

Table 2

Experimental Correlations of NuL for Air

Author	Correlation	Range of Re	B.C
Zukauskas [15]	$Nu_L = 0.4493\, Re_L$	40 – 1000	Isothermal
Morgan [16]	$Nu_L = 0.583 Re_L^{0.471}$	40 – 4000	Isothermal
Hilpert [17]	$Nu_L = 0.615\, Re_L^{0.466}$	40 – 4000	Isothermal
Knudsen and Katz [18]	$Nu_L = 0.683 Re^{0.466} Pr^{1/3}$	40 – 4000	Isothermal

The values of average Nusselt number are calculated from these correlations and are compared with the results of present study for Reynolds number ranging from 50 – 600. The results are presented in Table 3 and Fig 5. The analytical results obtained by Khan et al. [4] are also plotted. Present study is in close agreement with all previous experimental and analytical studies.

TABLE 3
Values of Nu_L Obtained From Correlations and Our Results at $50 \leq Re \leq 600$

Reynolds Number	**Zukauskas [15]**	**Morgan [16]**	**Hilpert [17]**	**Knudsen and Katz [18]**	**Khan [4]**	**Present Study**
50	Experimental	Experimental	Experimental	Experimental	Analytical	Numerical
100	3.18	3.68	3.81	3.83	3.7	3.82
200	4.49	5.10	5.26	5.29	5.2	5.15
300	6.35	7.07	7.26	7.31	7.4	7.12
400	7.78	8.56	8.77	8.83	9.0	8.59
500	8.99	9.80	10.03	10.10	10.3	9.97
600	10.05	10.89	11.13	11.20	11.5	11.17
	11.01	11.86	12.12	12.20	12.5	12.28

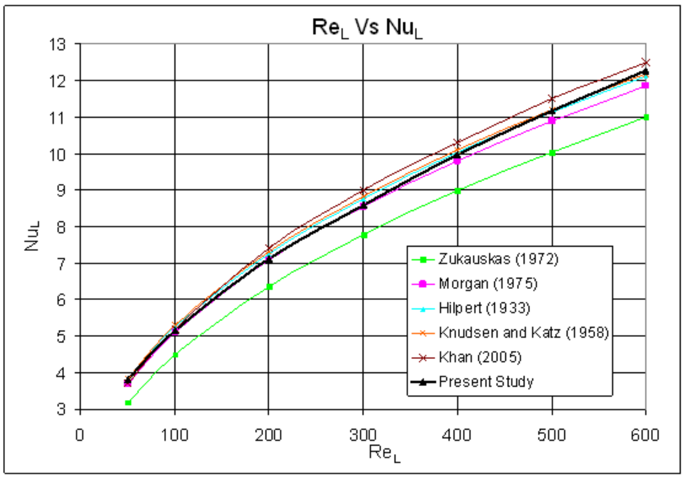

Figure 4: Comparison of NuL Vs ReL

It can be clearly seen from Fig 4 that as the Reynolds number increases, Nusselt number also increases. The increase in Reynolds number is brought about only by an increase in the free stream velocity as all the other parameters are kept constant. The increased velocity will increase the average heat transfer coefficient around the cylinder which eventually increases the average Nusselt number.

- **Local Nusselt Number**

Figure 5 shows the plot of Nusselt number at the stagnation point and is compared with the results given by Kays, Crawford and Weigand [19]. Again a good agreement is found with the previous study.

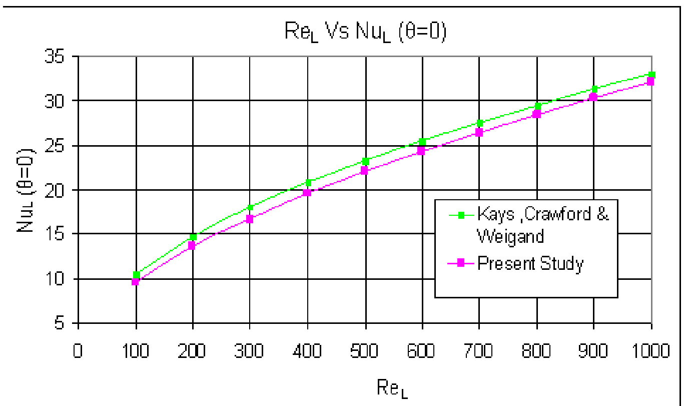

Figure 5: Comparison of ReL Vs NuL (θ=0)

Corresponding Author: M. JibranHaider (NJES10030131)

The variation of local Nusselt number along the cylinder is presented in Figs 6 and 7 in comparison with the results of Krall and Eckert [20] for Reynolds numbers 100 and 200. Krall and Eckert kept the same boundary condition of no slip and uniform wall temperature on the cylinder as is done in the present study.

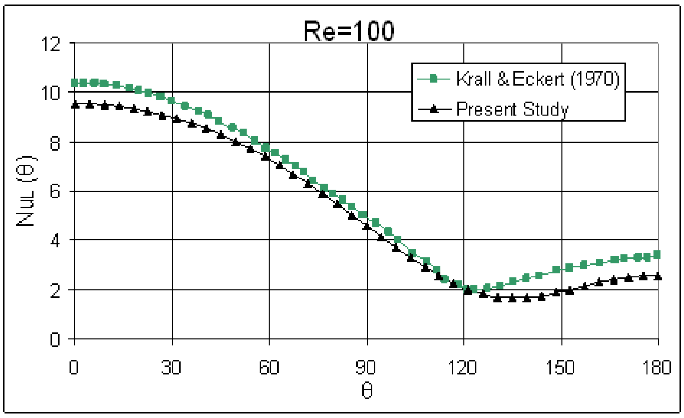

Figure 5: Comparison of ReL Vs NuL (θ=0)

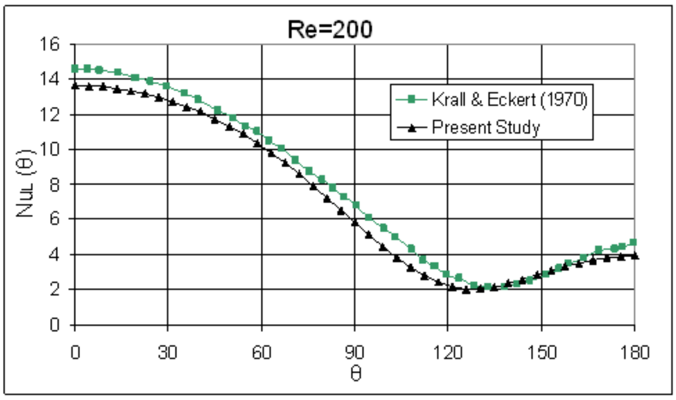

Figure 7: Variation of NuL (θ) at Re=200

Again the results are in good agreement. In both the graphs presented above, the values obtained by Krall and Eckert are slightly higher than the present study. The possible reason of deviation may be related to a higher blockage factor in the study of former authors. Present study is based on a blockage factor of 0.05.

- **Local Pressure Coefficient**

The analytical results of local pressure coefficient along the surface of the cylinder have been provided by Zdravkovich [21]. He has reported the results of Kawaguti and Apelt. Figure 8 provides a comparison of those results with present study at Reynolds number of 40.

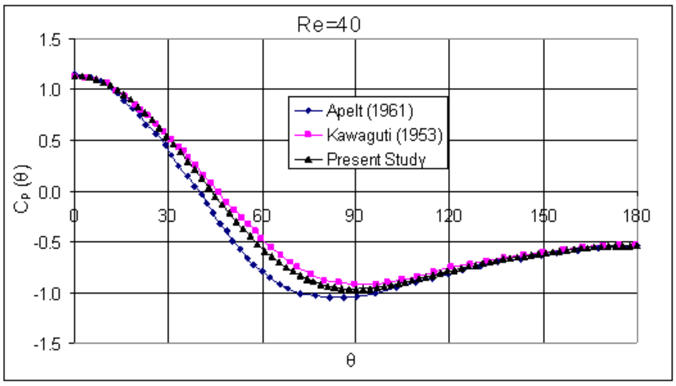

Figure 8: Variation of Cp (θ) at Re=40

An excellent agreement with the analytical results is observed. Experimental study over cylinders at such low Reynolds number yields a greater percentage of error. Therefore, the significance of analytical and numerical study at low Reynolds number is much more feasible. Similarly, Zdravkovich [20] has reported the results of Thoman & Szewczyk who carried out a computational study of flow over a circular cylinder. The results at a Reynolds number of 200 are compared with the study and found to be very close.

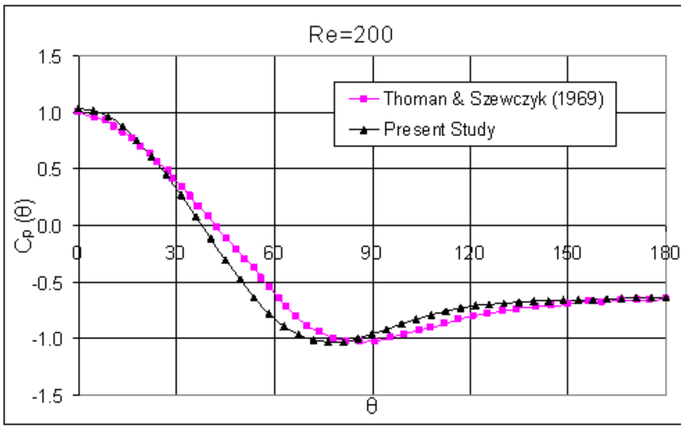

Figure 9: Variation of Cp (θ) at Re=200

B. Flow over an Inline Array of Cylinders

The next stage of analysis was to simulate flow over circular cylinders placed in an inline configuration as shown in Fig 10. Results were first obtained for 4 cylinders placed in a 2 x 2 array for which the longitudinal and transverse distances between the cylinders were kept at 2 times the diameter of the cylinder. Later flow over 25 cylinders placed in a 5 x 5 array was simulated.

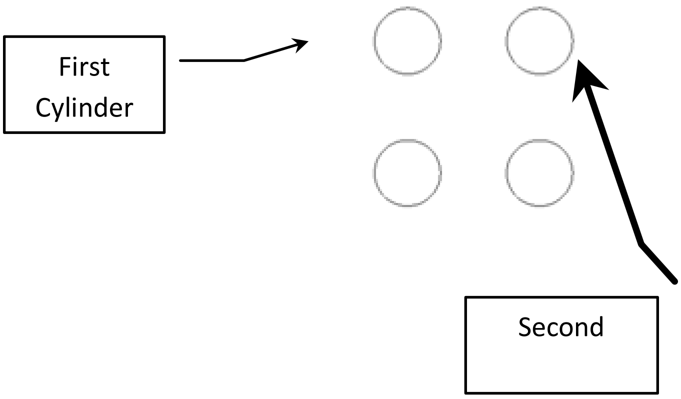

Figure 10: Four Cylinders Placed in an Inline Arrangement

- **Local Nusselt Number**

Distribution of local Nusselt number has been obtained for the inline configuration. The results are compared with that of Buyruk [12] for a Reynolds number of 200 and shown in Figs 11 and 12 for upstream and downstream cylinders. A very good agreement is observed for both the cylinders.

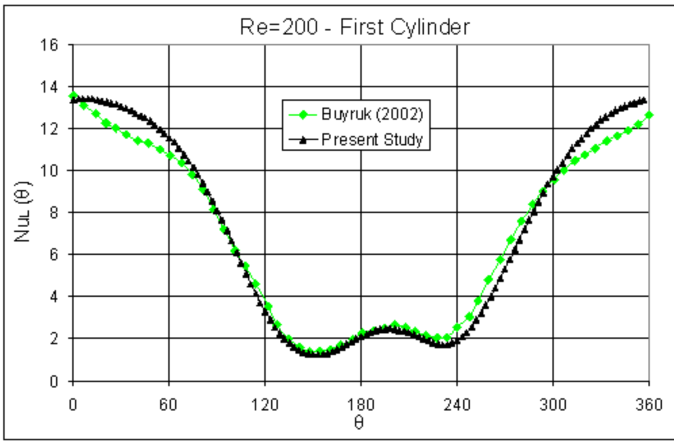

Figure 11: Variation of Nu_L (θ) at Re=200 along the First Cylinder

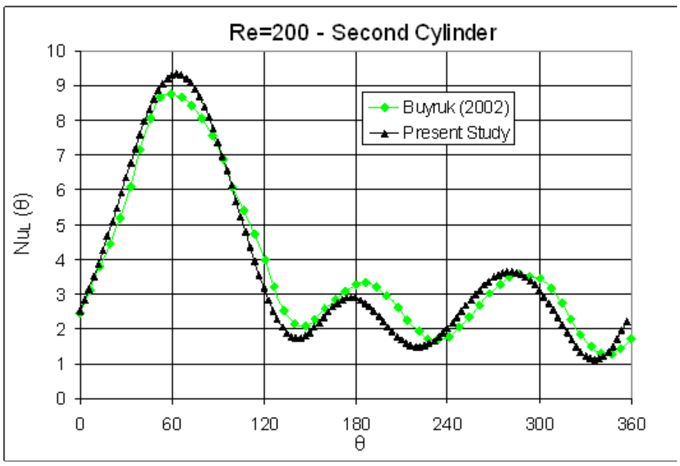

Figure 12 Variation of Nu_L (θ) at Re=200 along the Second Cylinder

- **Contours of Static Pressure and Velocity**

The contours of static pressure are shown in Fig 13 at a Reynolds number of 200 around the cylinders. The shifting of the front stagnation points on the front cylinders (red region) and the rear cylinders (green region) is evident. This is due to the venturi effect created between the two rows of cylinders which creates suction and shifts the front stagnation point.

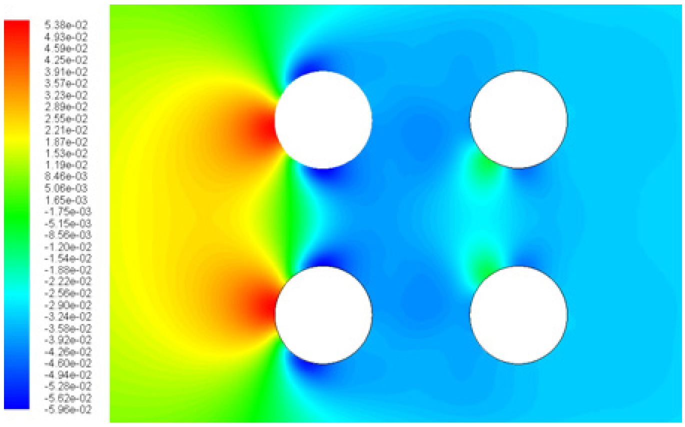

Figure 13: Contours of Static Pressure at Re=200

Velocity contours are also shown below at a Reynolds number of 40 and 200.

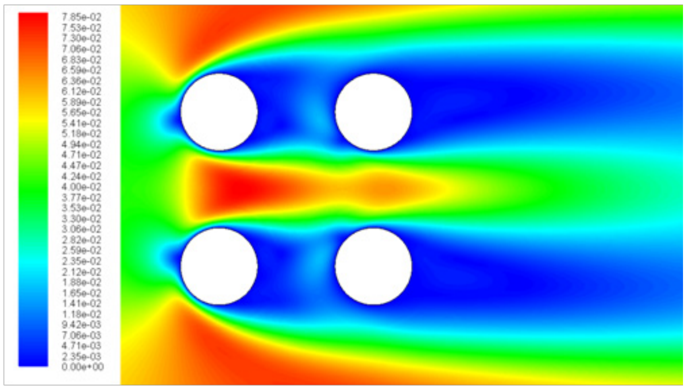

Figure 14: Contours of Velocity at Re=40

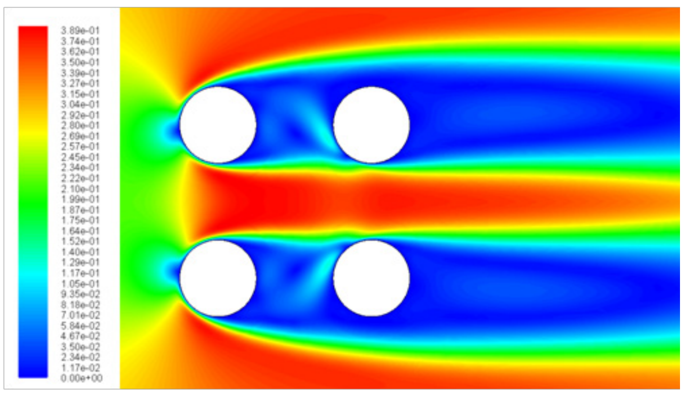

Figure 15: Contours of Velocity at Re=200

Corresponding Author: M. JibranHaider (NJES10030131)

The increase in velocity between the cylinders as Reynolds number increases is shown by the red region. The waves generated by the cylinders at the front are disturbed due to the presence of rear cylinders. The disturbance is much greater at a Reynolds number of 200 than at 40.

- **Average Nusselt Number**

The results of average Nusselt Number were obtained for the inline array of 5 by 5 and are presented in Table 4. The longitudinal and transverse distances were kept at 2.5 times the diameter of the cylinder.

Table 4
Variation of Nu with Re for a 5 x 5 Inline Array

Reynolds Number	**Nu**
100	3.005
500	6.907
1000	11.277
2000	18.064
3000	23.453
4000	28.192
5000	33.175
6000	38.235
7000	43.581
8000	49.150
9000	54.433
10000	59.462

- **Contours of Temperature**

The contours of temperature are shown below for various Reynolds numbers.

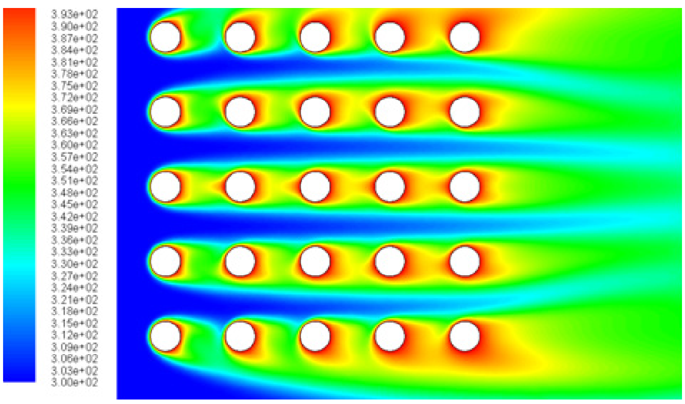

Figure 16 Contours of Temperature at Re=100

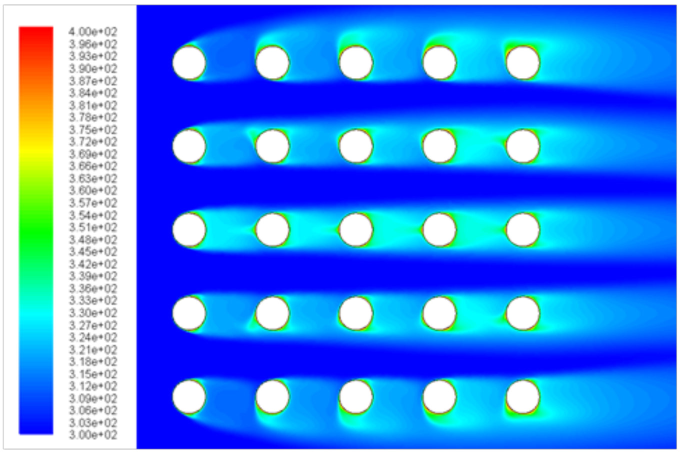

Figure 18 Contours of Temperature at Re=5000

The plots above show the decrease in the thermal boundary layer as Reynolds number increases from 100 to 1000 and finally to 5000. So the temperature gradient at a higher Reynolds number is very steep which gives better heat transfer. It is also evident that the diffusion of temperature contours occurs much early downstream of the cylinders at a lower Reynolds numbers. Lastly, the symmetry of temperature contours can be observed about the central row. It is to be noted that there is no shift in the stagnation points of the cylinders present in the central row while every other cylinder experiences some change in stagnation point.

C. Flow over a Staggered Array of Cylinders

The flow was also simulated over a staggered array of 3 cylinders as shown in Fig 19 and then for 23 cylinders. The longitudinal and transverse pitches for the three cylinders are kept 2 .

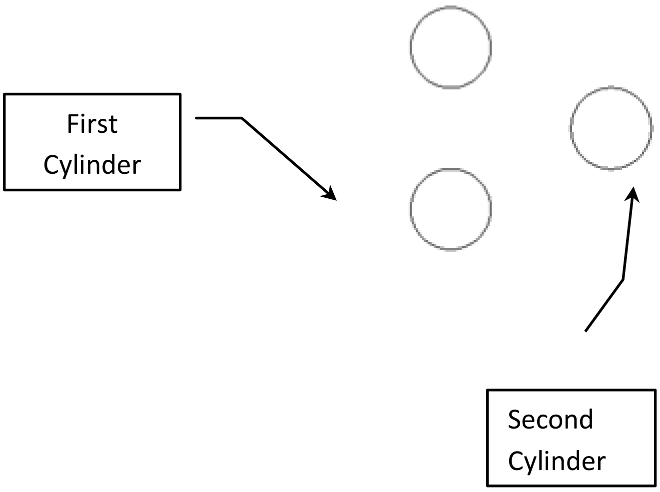

Figure 19: Three Cylinders Placed in a Staggered Arrangement

- **Local Nusselt Number**

Variation of local Nusselt number is obtained and compared with the results of Buyruk [12]. The comparison is shown in Figs 20 and 21 at a Reynolds number of 200 for the first and second cylinders.

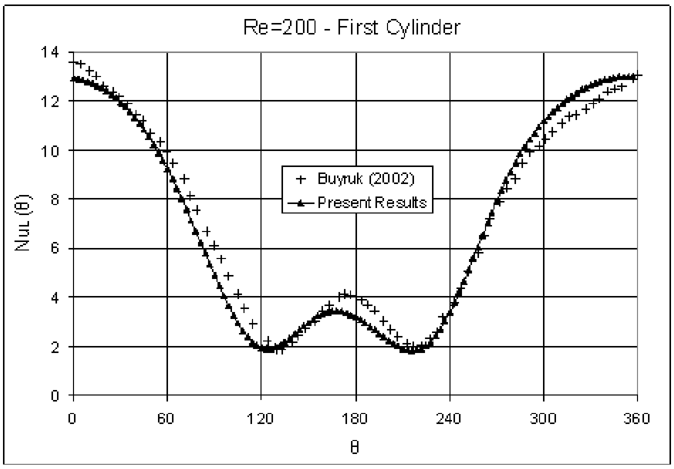

Figure 20: Variation of NuL (θ) at Re=200 along the First Cylinder

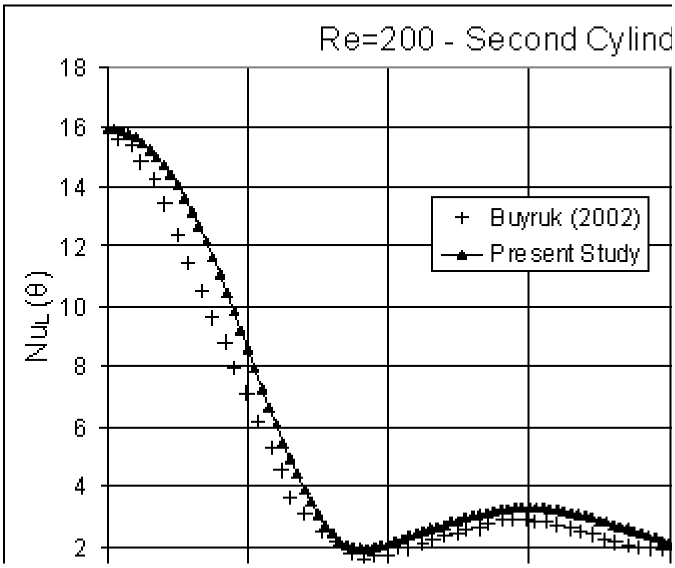

Figure 21: Variation of NuL (θ) at Re=200 along the Second Cylinder

A close examination of the plot reveals that the values of local Nusselt number obtained by Buyruk for the second cylinder are not exactly symmetrical over the upper and lower surfaces. The configuration of the cylinders is such that flow should be symmetrical for the second cylinder. On the other hand, our results are exactly symmetrical.

- **Contours of Static Pressure and Velocity**

The contours of static pressure are shown in Fig 22 at a Reynolds number of 120. The shifting of the front stagnation points is clearly visible on the two cylinders at the front. As expected symmetrical pressure contours are obtained for the second cylinder.

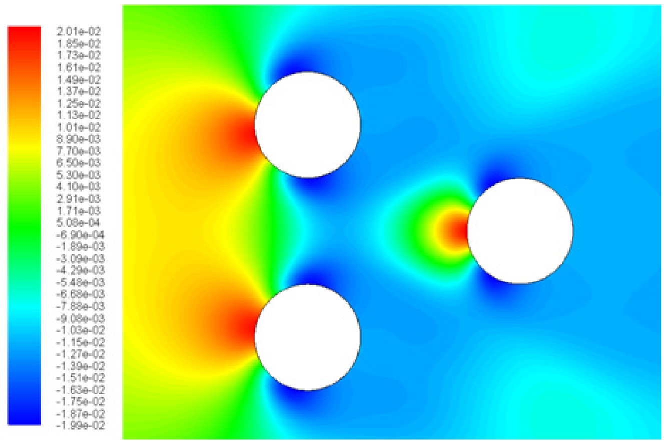

Figure 22: Contours of Static Pressure at Re=120

The contours of velocity at Reynolds number 40 and 500 are shown in the following figures

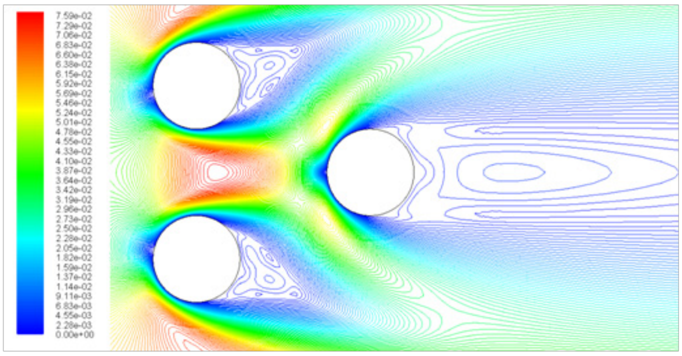

Figure 23: Contours of velocity at Re =40

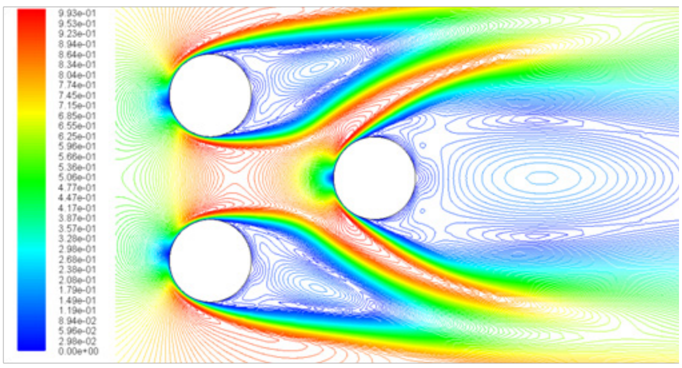

Figure 24: Contours of Velocity at Re=500

It can be clearly seen that at a higher Reynolds number separation of the boundary layer from all three cylinders occurs early. Therefore, the waves created in Fig 24 are much greater than those in Fig 23.

Corresponding Author: M. JibranHaider (NJES10030131)

- **Average Nusselt Number**

Flow is simulated over a staggered array of 23 cylinders. Longitudinal and transverse pitches are kept at 2.5 each. The results of average Nusselt numbers are obtained for various Reynolds Numbers.

Table 5
Variation of Nu with Re for a Staggered Array

Reynolds Number	Nu
100	3.470
500	9.941
1000	14.875
2000	22.346
3000	28.661
4000	34.495
5000	40.432
6000	46.784
7000	54.304
8000	61.821
9000	68.310
10000	74.671

- **Contours of Temperature**

The contours of temperature are shown in Figs 25, 26 and 27 at different Reynolds numbers.

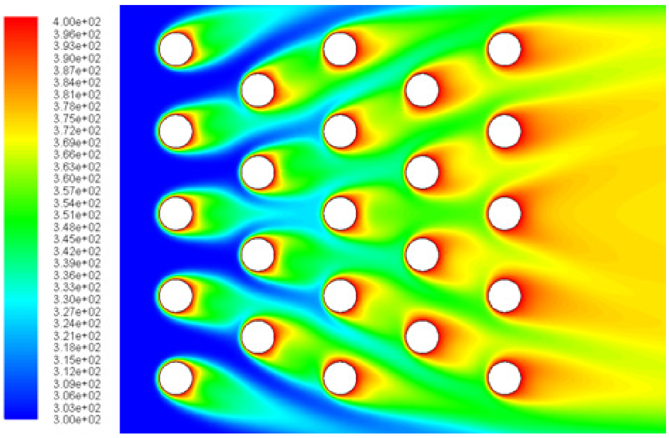

Figure 25: Contours of Temperature at Re=100

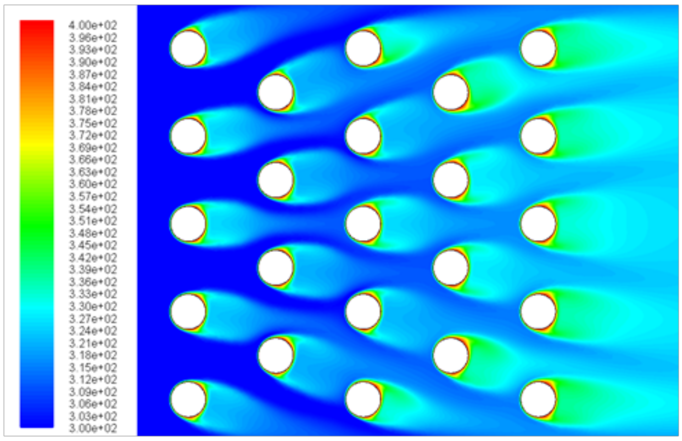

Figure 26 Contours of Temperature at Re=1000

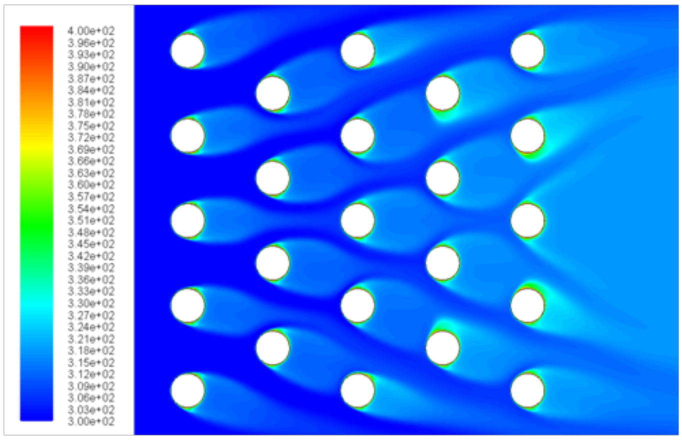

Figure 27 Contours of Temperature at Re=5000

As the Reynolds number increases from 100 to 5000, the thickness of the thermal boundary layer decreases significantly. Therefore, the temperature gradient at Reynolds number 5000 is much greater than that at Reynolds numbers 1000 or 100. This high temperature gradient is responsible for the increased heat transfer as Reynolds number increases. As in the case of an inline array, the symmetry of temperature contours can also be observed for a staggered array about the central row.
Figure 28 shows a comparison of the Nusselt number for inline and staggered arrays.

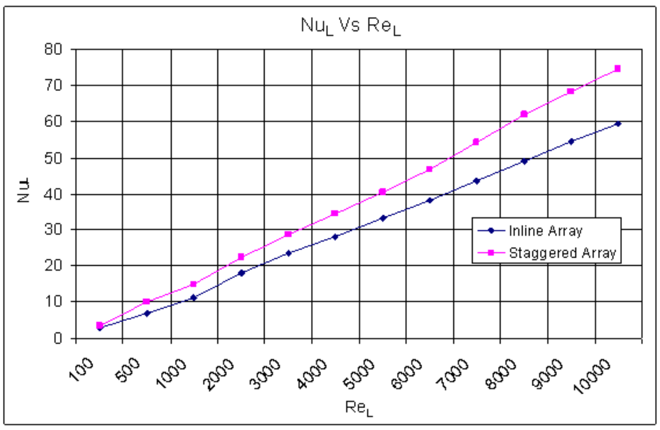

Figure 28: Variation of NuL Vs ReL for Inline and Staggered Arrays

It can be concluded that the heat transfer from a staggered array is higher than that from an inline array when subjected to the same Reynolds number. This is also confirmed by the temperature contours of the two arrangements as the diffusion of contours is more intense in the staggered array as compared to the inline array.

Conclusions

Numerical study has been undertaken to analyze heat transfer and flow characteristics past a single cylinder, inline array and staggered array at various Reynolds numbers. It can be concluded from the results that:

1. Heat transfer from a staggered array of cylinders is slightly higher than that from an inline array of cylinders.
2. The simulated results of local Nusselt number, average Nusselt number and local pressure coefficient from circular cylinders are in good agreement with the analytical, experimental and numerical results available in existing literature.

REFERENCES

1. V. D. H. Zijnen, “Modified correlation formulae for the heat transfers by natural and by forced convection from horizontal cylinders”, Appl. Sci. Res, Vol. 6, 1956, pp. 129–140.
2. G. R. Ahmed and M. Yovanovich, “Analytical method for forced convection from flat plates, circular cylinders and spheres”, Journal of Thermophysics and Heat Transfer, Vol. 9, No. 3, 1995, pp. 516–523.
3. W. A. Khan, J. Culham, and M. Yovanovich, “Fluid flow and heat transfer from a pin fin: analytic approach”, American Institute of Aeronautics and Astronautics, Vol. 163, 2003, pp. 1–12.
4. W. A. Khan, J. Culham and M. Yovanovich, “Fluid flow around and heat transfer from an infinite circular cylinder”, Journal of Heat Transfer, Vol. 27, 2005, pp. 785-790.
5. D. Meel, “A method for the determination of local convective heat transfer from a cylinder placed normal to an air stream”, Int. J. Heat Mass Transfer, Vol. 5, 1962, pp. 715–722.
6. T. Igarashi, “Characteristics of the flow around two circular cylinders arranged in tandem”, JSME, Vol. 24, No. 188, 1981, pp. 323–331.
7. T. Igarashi, “Characteristics of a flow around two circular cylinders of different diameters arranged in tandem”, JSME, Vol. 25, 1982, pp. 349–357.
8. T. Igarashi and K. Suzuki, “Characteristics of the flow around three circular cylinders arranged inline”, JSME, Vol. 27, 1984, pp. 2397–2404.
9. E. Buyruk, “Heat transfer and flow structures around circular cylinders in cross flow”, Tr. Journal of Engineering and Environmental Science, Vol. 23, 1997, pp 299–315.
10. M. Mehrabian, “Heat transfer and pressure drop characteristics of cross flow of air over a circular tube in isolation and/or in a tube bank.”, The Arabian Journal for Science and Engineering, Vol. 32, No. 2B, 2005, pp. 365–376.
11. T. Wung and C. Chen, “Finite analytic solution of convective heat transfer for tube arrays in cross flow”, Journal of Heat Transfer, Vol. 111, 1989, pp. 633–648.
12. E. Buyruk, “Numerical study of heat transfer characteristics on tandem cylinders, inline and staggered tube banks in cross flow of air”, Int. Comm. Heat Mass Transfer, Vol. 29, No. 3, 2002, pp. 355–366.
13. K. Szczepanik, A. Ooi1, L. Aye and G. Rosengarten, “A numerical study of heat transfer from a cylinder in cross flow”, Proceedings of 15th Australasian Fluid Mechanics Conference, Sydney, December 13-17, 2004.
14. “FLUENT 6.3 User’s Guide” , 2006.
15. A. Zukauskas, “Advances in heat transfer”, Academic Press New York, 1972, pp. 93-160.
16. V. Morgan, “The overall convective heat transfer from smooth circular cylinders”, Advances in Heat Transfer, Vol.11, Academic Press, New York, 1975, pp. 199–264.
17. R. Hilpert, “Warmeabgabe von geheizten drahten und rohren”, Forch. Geb. Ingenieurwes, Vol. 4, 1933, pp. 215–224.
18. J. Knudsen and D. Katz, “Fluid Dynamics and Heat Transfer”, McGraw Hill, New York, 1958.
19. Kays, W. Crawford and B. Weigand, “Convective Heat and Mass Transfer”, 4th Edition McGraw-Hill, 2005.
20. K. Krall and E. Eckert, “Heat transfer to a transverse circular cylinder at low Reynolds Numbers including rarefaction effects”, Fourth International Heat Transfer Conference”, Vol. 3, 1970, pp. 1–11.
21. M. Zdravkovich, “Flow around circular cylinders”, Vol. 1, 1997, pp. 260–273.

Corresponding Author: M. JibranHaider (NJES10030131)